C h a p t e r 3

Impacts of the Graft Polymer Architecture on Physical Properties

1. Chang, A. B.;[+] Lin, T.-P.;[+] Thompson, N. B.; Luo, S.-X.; Liberman-Martin, A. L.; Chen, H.-Y.; Grubbs, R. H. Design, Synthesis, and Self-Assembly of Polymers with Tailored Graft Distributions. *J. Am. Chem. Soc.* **2017**, *139*, 17683–17693. ([+]*Equal contributions.*)

2. Lin, T.-P.;[+] Chang, A. B.;[+] Luo, S.-X.; Chen, H.-Y.; Lee, B.; Grubbs, R. H. Effects of Grafting Density on Block Polymer Self-Assembly: From Linear to Bottlebrush. *ACS Nano* **2017**, *11*, 11632–11641. ([+]*Equal contributions.*)

3. Haugan, I. N.; Maher, M. J.; Chang, A. B.; Lin, T.-P.; Grubbs, R. H.; Hillmyer, M. A.; Bates, F. S. Consequences of Grafting Density on the Linear Viscoelastic Behavior of Graft Polymers. *ACS Macro Lett.* **2018**, *7*, 525–530.

ABSTRACT

Living ring-opening metathesis polymerization (ROMP) enables precise control over the graft polymer architecture. In this chapter, we will discuss the physical consequences of varying the molecular architecture in two contexts: block polymer self-assembly and linear rheology. The impacts of grafting density and graft distribution on block polymer self-assembly will be first described. AB graft diblock polymers with tapered, uniform, and inverse-tapered molecular "shapes" were synthesized by ROMP. Small-angle X-ray scattering (SAXS) analysis of the self-assembled structures indicates that the graft distribution influences shape-filling demands and therefore the backbone conformation. Across seventeen series of uniformly grafted block polymers spanning the linear, comb, and bottlebrush regimes ($0 \leq z \leq 1$), the scaling of the lamellar period with the total backbone degree of polymerization ($d^* \sim N_{bb}^{\alpha}$) was studied. The scaling exponent α monotonically decreases with decreasing grafting density (z) and exhibits an apparent transition at a critical $z \approx 0.2$, suggesting significant changes in the chain conformations. In complementary studies, the linear viscoelastic behavior of eight series of graft homopolymers was investigated as a function of grafting density ($0 \leq z \leq 1$) and backbone length ($10 < N_{bb} < 3000$). Dynamic master curves reveal that these polymers display Rouse-

like and reptation dynamics with a sharp transition in the zero-shear viscosity data, demonstrating that grafting density strongly impacts the onset of entanglements. The scaling of the entanglement plateau modulus with *z* was found to conflict with existing theoretical models for graft polymers, but a molecular interpretation based on thin flexible chains at low *z* and thick semiflexible chains at high *z* anticipates the sharp transition between the limiting dynamic regimes. Collectively, the behavior disclosed herein provides valuable insights into the static and dynamic impacts of the graft polymer architecture, enabling comparisons with existing theory and introducing new opportunities for materials design.

Table of Contents

3-1 Impact of Graft Distribution on Block Polymer Self-Assembly

Grafting density and graft distribution are important parameters that govern polymer architectures and physical properties. We recently developed a grafting-through ring-opening metathesis copolymerization approach to tune the grafting density and graft distribution (Chapter 2). In this section, we will further demonstrate the utility of the ROMP method by describing the synthesis of AB diblock polymers with variable side chain distributions, then examine how differences in chain connectivity affect self-assembly.

Three different AB graft diblock polymers were synthesized by controlled ROMP. Simple substitutions of the discrete co-monomers ensure that the block polymers differ *only* in the distribution of the grafts. All other aspects of the structure and chemistry are identical:

- All block polymers feature PDMS and PS side chains. The grafting-through approach guarantees that the side chain molecular weights are the same within each block (**PDMS**: 1280 g mol^{-1}, **PS**: 3990 g mol^{-1}).
- The grafting density in each block is 50%.
- The backbone degree of polymerization in each block is the same. For the A block (**PDMS** + diluent), $N_{bb,A} = 150$; for the B block (**PS** + diluent), $N_{bb,B} = 50$.
- The above constraints enforce equal block volume fractions for all three block polymers: $f = 0.50$.

The side chain distributions can be varied while fixing all of the preceding parameters by switching the identity of the diluents in each block. Scheme 3.1 illustrates the resulting block polymer structures with uniform (**BP-1**) or gradient (**BP-2**, **BP-3**) graft distributions. The backbones are drawn in the fully extended limit for ease of visualization, and the side chain conformations and cross-sectional radii are depicted as anticipated by existing theory.[1-4]

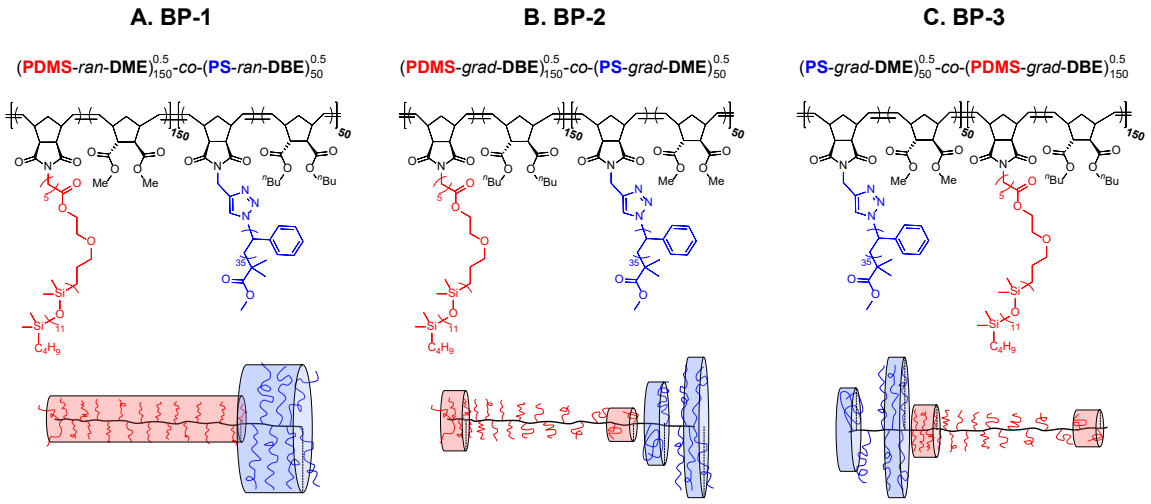

Scheme 3.1: Illustrations of three AB graft diblock polymers differing only in the side chain distribution: (*A*) uniform (**BP-1**), (*B*) gradient (**BP-2**), and (*C*) inverse-gradient (**BP-3**). (*top*) Chemical structures. (*bottom*) Schematic illustrations of the anticipated molecular "shapes," shown in the limit of fully extended backbones for ease of visualization.

BP-1 was synthesized by first copolymerizing **PDMS** and *endo,exo*-norbornenyl dimethylester (*dx*-DMeE, **1a**) in a 1:1 feed ratio. Since $r_1 = 1.1$ and $r_2 = 0.94$, the first block has an ideal random backbone sequence and therefore uniform side chain distribution.

After complete consumption of **PDMS** and *dx*-DMeE, the chain ends were still living, and the second block (B) was added via a 1:1 mixture of **PS** and *endo,exo*-norbornenyl di-*n*-butylester (*dx*-D^{n}BuE, **1d**). Since $r_1 = 0.80$ and $r_2 = 1.2$, the side chain distribution in the second block is also effectively uniform. A graft polymer with a gradient side chain distribution (**BP-2**) was synthesized by keeping all conditions exactly the same but simply switching the diluents. The first block (A) was synthesized by copolymerizing **PDMS** with *dx*-D^{n}BuE instead of *dx*-DMeE; since $r_1 = 1.1$ and $r_2 = 0.43$, the block is rich in the macromonomer at early conversions and rich in the diluent at late conversions. Addition of **PS** + *dx*-DMeE as the second block (B; $r_1 = 0.54$, $r_2 = 1.4$) therefore produces a block polymer with low grafting density at the block-block junction and increasing grafting density moving toward the free chain ends. A third distinct graft block polymer (**BP-3**) was synthesized by keeping all conditions exactly the same as those for **BP-2** but simply switching the order in which the blocks were added. By polymerizing block B (**PS** + *dx*-DMeE) first and block A (**PDMS** + *dx*-D^{n}BuE) second, the product features the inverse-tapered architecture compared to **BP-2**. Scheme 3.1 provides the chemical structures of **BP-1**, **-2**, and **-3**. Analysis by SEC (Appendix B, Figure B.2) and ^{1}H NMR (Figure B.3) confirms that their overall molecular weights and chemical compositions are identical.

The three graft block polymers were annealed for 24 hours at 140 °C under vacuum and modest applied pressure. The resulting microphase-separated structures were characterized by synchrotron-source small-angle X-ray scattering (SAXS). Comparison of the SAXS patterns (Figure 3.1) indicates that all three samples form long-range-ordered lamellar morphologies but also reveals two crucial differences. First, the lamellar periods ($d^* = 2\pi/q^*$) differ. Equal values of d^* are perhaps expected since the chemical compositions and backbone and side chain lengths are all identical; on the contrary, **BP-1** exhibits $d^* = 51.0$ nm (Figure 3.1A), while **BP-2** (3.1B) and **BP-3** (3.1C) exhibit $d^* = 49.5$ and 46.5 nm, respectively. Second, the relative thicknesses of the A and B domains (d_A and d_B) also differ. Compared to **BP-1**, **BP-2** forms more symmetric lamellae, as evidenced by the weak intensities of the even-order diffraction peaks (q_2, q_4, …). The inverse-gradient **BP-3** forms lamellae that are the most symmetric of all; in fact, the complete extinction of even-order peaks suggests that d_A and d_B are equal.

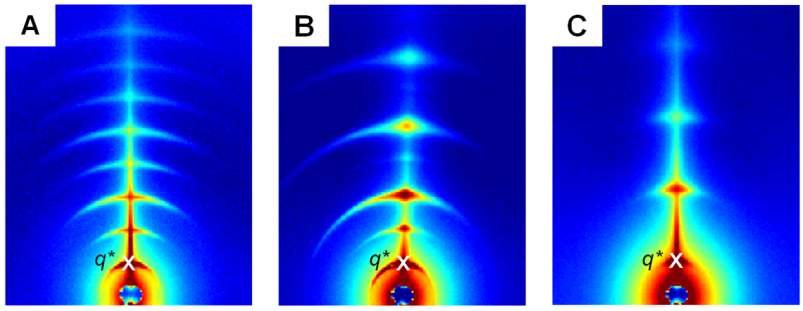

Figure 3.1: SAXS patterns corresponding to the annealed graft block polymers: (*A*) **BP-1**, (*B*) **BP-2**, (*C*) **BP-3**. The white "x"' indicates the first-order diffraction peak, q^*.

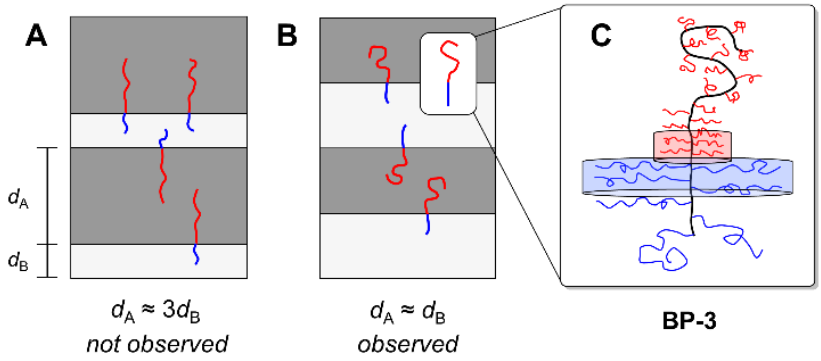

Figure 3.2: Schematic illustration of the relationships between chain dimensions and the lamellar period. (*A*) $d_A \approx 3d_B$ is expected if the backbones are fully stretched (since $N_{bb,A} = 3N_{bb,B}$), but it is consistent with SAXS data. (*B*) Instead, $d_A \approx d_B$ is observed. This requires bending of the A block backbone. (*C*) Illustration of **BP-3** and revised chain conformations.

This symmetry is perhaps surprising: although the block volume fractions are equal ($f = 0.50$), the backbone lengths are highly asymmetric: $N_{bb,A} = 3N_{bb,B}$. The graft polymer backbones are clearly not fully extended as illustrated in Scheme 3.1. If the backbone were fully extended, $d_A = 3d_B$ is expected for all samples (Figure 3.2A). Every fourth diffraction peak (q_4, q_8, …) would be weak, which is *inconsistent* with the SAXS data. Figure 3.3 compares simulated and measured 1D-averaged SAXS data for **BP-3**, supporting the assignment of symmetric layer structures instead ($d_A = d_B$, Figure 3.2B). The SAXS data indicates that the backbones are flexible and that changing the side chain distribution affects the backbone conformation. Gradient distributions in which the grafting density is *either* lowest (**BP-2**) or highest (**BP-3**) at the block-block junction enable more efficient packing than uniform distributions (**BP-1**). Closer packing balances the backbone

asymmetry with the demands of equal block volumes, most likely via bending of the A (PDMS) block backbone (Figure 3.2C).

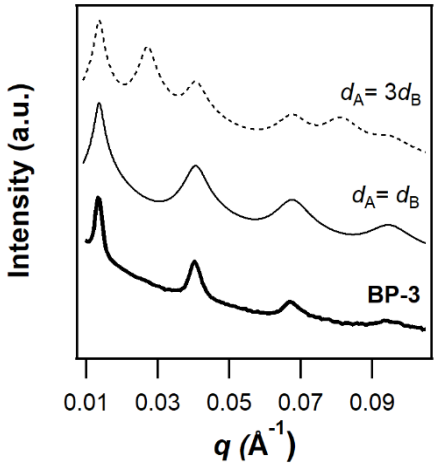

Figure 3.3: Comparison of simulated (*top, middle)* and measured (*bottom*) 1D-averaged SAXS data. The experimental data closely matches the expected SAXS pattern corresponding to lamellae with symmetric ($d_A = d_B$) domains.

For all samples, the backbones should be strongly stretched at the domain interface as a consequence of segregation. In the case of **BP-2**, the chains should have the highest local backbone stiffness but also the greatest free volume at the free chain ends. Compared to the uniformly grafted **BP-1**, this may better accommodate high grafting density in the center of the domains. In the case of **BP-3**, since the backbones are already strongly stretched at the domain interfaces, the high grafting density may not significantly stretch the backbones further, resulting in the smallest d^* among all three graft polymers. Low grafting density at the free chain ends should result in comparatively low backbone stiffness and therefore better accommodate bending in the A block (Figure 3.2C). Collectively, these results indicate that the side chain distribution affects chain stretching and packing. This result indicates that molecular "shape" is indeed an important design parameter, allowing materials to possess non-equilibrium density distributions.

3-2 Impact of Grafting Density on Block Polymer Self-Assembly

3-2.1 Introduction

We recently reported the efficient synthesis of graft polymers with controlled grafting density (z), defined as the average number of polymer side chains per backbone repeat unit (Chapter 2). In this section, we will discuss the effects of grafting density on the scaling of the lamellar period (d^*) with the total backbone degree of polymerization (N_{bb}). The scaling of d^* reflects steric demands and penalties to chain stretching, thus providing valuable insight into the physical consequences of varying polymer architectures. d^* is an attractive parameter to study because it has an unambiguous physical definition (unlike potentially model-dependent parameters such as χ) and can be directly measured by scattering and electron microscopy.[5]

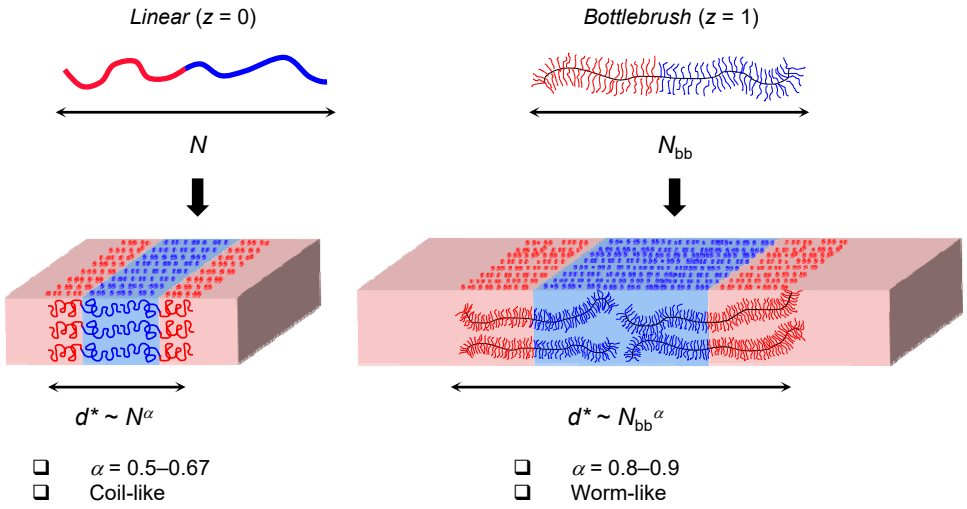

Figure 3.4: Self-assembly of linear and bottlebrush diblock polymers into lamellae.

Figure 3.4 illustrates the self-assembly of linear (z = 0) diblock polymers into lamellar morphologies. For symmetric linear diblock polymers, arguments based on free energy demands accurately predict the scaling behavior ($d^* \sim N_{bb}^{\alpha}$). The scaling exponent α is 1/2 in the weak segregation limit ($\chi N_{bb} \approx 10.5$) and plateaus at 2/3 in the strong segregation limit ($\chi N_{bb} >> 10.5$).[6-7] The small scaling exponent is inherently related to the coil-like chain conformations. In contrast, reports of scaling behavior for block polymers with bottlebrush (z = 1) and other complex, non-linear architectures are limited due to the

synthetic challenges associated with (1) precisely controlling the architecture, molecular weight, and composition and (2) efficiently preparing multiple samples to study trends.

Bottlebrush polymers have recently emerged as an advanced class of non-linear architectures that manifest unique physical, mechanical, and dynamic properties.[8-15] Like their linear analogues, bottlebrush diblock polymers can access lamellar morphologies (Figure 3.4). However, bottlebrush block polymers display much larger scaling exponents (α = 0.8–0.9),[16-19] consistent with extended backbone conformations. Steric repulsion between the densely grafted side chains imparts a certain bending rigidity to the backbone, which can be modeled as a wormlike chain.[20-23] The unique properties of bottlebrush polymers have been previously exploited for applications in photonics,[24-27] lithography,[28-29] and surface coatings.[30] For example, the bottlebrush architecture minimizes chain entanglement and promotes rapid self-assembly to structures with ultra-large d^*, enabling the fabrication of photonic materials that reflect visible and even infrared radiation. In contrast, such materials are generally inaccessible using linear and low-z analogues due to the ultra-high molecular weights required as well as their low entanglement molecular weights.

The effects of grafting density on the rheological properties of homopolymers have received tremendous interest.[31-39] However, the impacts of grafting density on block polymer self-assembly have not been explored.[40-43] Elucidating these physical principles is not only of fundamental importance but should also guide material design. With this mindset, we launched the study on block polymers with systematically modified grafting densities ($0 \leq z \leq 1$) spanning the linear, comb, and bottlebrush regimes. The self-assembly of these block polymers was examined by small-angle X-ray scattering (SAXS), allowing determination of the scaling behavior. These studies reveal vital information on the backbone conformations, and the determined scaling laws allow the prediction of lamellar periods toward improved materials design.

*3-2.2 Synthesis of Block Polymers with Variable Grafting Density (**System I**)*

Ring-opening metathesis polymerization (ROMP) is a powerful strategy to synthesize well-defined bottlebrush polymers.[44-47] We targeted poly(D,L-lactide)-*b*-polystyrene (**PLA**-*b*-**PS**) graft diblock polymers to permit comparisons with brush PLA-*b*-

PS systems previously investigated in the context of self-assembly.[17-19,27,48] All polymerizations were performed in CH_2Cl_2 at room temperature under inert atmosphere. To vary the grafting density (Scheme 3.2), the first block was synthesized by copolymerizing a **PLA** macromonomer (M_n = 3230 g/mol) with a discrete co-monomer (*i.e.*, diluent), **DME** (*endo*,*exo*-norbornenyl dimethyl ester, M_n = 210 g/mol). As discussed in Chapter 2-7, the grafting density (z) is precisely determined by the feed ratio according to Eq. 3-1:

$$z = \frac{[\mathbf{PLA}]_0}{[\mathbf{PLA}]_0 + [\mathbf{DME}]_0} \qquad \text{Eq. 3-1}$$

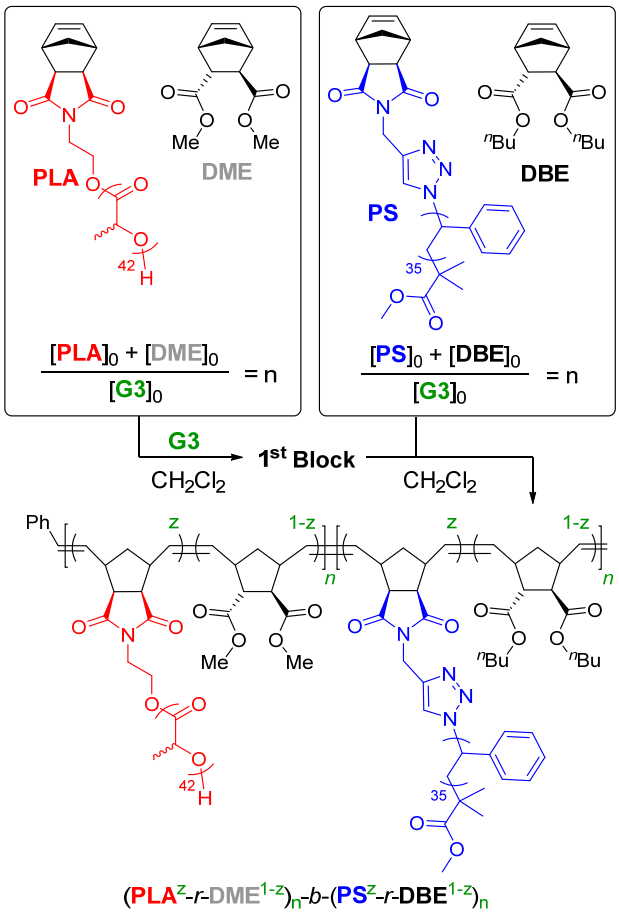

Scheme 3.2: Synthesis of (**PLA**^{z}-*r*-**DME**$^{1-z}$)$_n$-*b*-(**PS**^{z}-*r*-**DBE**$^{1-z}$)$_n$ block polymers (**System I**) featuring variable backbone degrees of polymerization ($N_{bb} = 2n$ = 44–363) and grafting densities (z = 1.00, 0.75, 0.50, 0.35, 0.25, 0.20, 0.15, 0.05, 0).

After both co-monomers were fully consumed (verified by ^{1}H NMR), a mixture of a **PS** macromonomer (M_n = 3990 g/mol) and another discrete diluent, **DBE** (*endo*,*exo*-norbornenyl di-*n*-butyl ester, M_n = 294 g/mol), was introduced as the second block. The **PS**/**DBE** feed ratio was the same as the **PLA**/**DME** feed ratio in the first block. The determined reactivity ratios (block A: r_{PLA} = 0.92, r_{DME} = 1.11; block B: r_{PS} = 0.80, r_{DBE} = 1.16) suggest that the copolymerization is statistically random with minimal compositional drift. (See Chapter 2-5.) Monitoring the instantaneous monomer concentrations over time indicates that the macromonomer and diluent are incorporated at approximately equal rates in each block, consistent with uniform z throughout the entire block polymer. The backbone degrees of polymerization (n) for the first and second blocks were equal and determined by the ratio of the total monomer concentration to catalyst (**G3**) concentration (Eqs. 3-2–3-3:

$$n = \frac{[\mathbf{PLA}]_0 + [\mathbf{DME}]_0}{[\mathbf{G3}]_0} = \frac{N_{bb}}{2} \qquad \text{Eq. 3-2}$$

$$n = \frac{[\mathbf{PS}]_0 + [\mathbf{DBE}]_0}{[\mathbf{G3}]_0} = \frac{N_{bb}}{2} \qquad \text{Eq. 3-3}$$

For **System I**, nine different series with variable grafting densities (z = 1.00, 0.75, 0.50, 0.35, 0.25, 0.20, 0.15, 0.05, and 0) were prepared. Each series includes five to seven block polymers with fixed composition and varying backbone lengths (N_{bb} = 44–363). To achieve consistent control over z, the targeted macromonomer/diluent feed ratios were verified by ^{1}H NMR prior to initiating the first block with **G3**. After reaching >99% conversion, the reaction mixtures were quenched by addition of excess ethyl vinyl ether. The block polymers were precipitated into methanol at −78 ℃, isolated by filtration, and dried under vacuum for >24 h. The first blocks and precipitated products were analyzed by NMR and size-exclusion chromatography (SEC), allowing determination of the molecular weights and therefore N_{bb}. These analyses indicated that our methodology produced well-defined, monodisperse ($Đ$ = 1.01–1.18) graft block polymers. The compositions of all samples in **System I** are presented in Table 3.1.

Table 3.1: Total number-average molecular weights (M_n) and total backbone degrees of polymerization (N_{bb}) (**PLA**^{z}-*r*-**DME**$^{1-z}$)$_n$-*b*-(**PS**^{z}-*r*-**DBE**$^{1-z}$)$_n$ graft block polymers (**System I**).

z	ID	M_n (kDa)	N_{bb}
1.00	A1	158	44
	A2	304	84
	A3	465	129
	A4	596	165
	A5	718	199
0.75	B1	234	84
	B2	361	130
	B3	467	168
	B4	606	219
0.50	C1	166	86
	C2	243	126
	C3	315	163
	C4	400	207
0.35	D1	124	87
	D2	181	127
	D3	238	167
	D4	301	211
	D5	369	258
	D6	430	301
0.25	E1	98.8	90
	E2	146	134
	E3	167	153
	E4	200	183
	E5	216	197
	E6	244	223
	E7	286	262
0.20	F1	119	128
	F2	153	166
	F3	195	211
	F4	216	234
	F5	230	249
	F6	248	268
	F7	294	318
0.15	G1	163	216
	G2	178	235
	G3	189	250
	G4	216	286
	G5	232	307
	G6	246	325
0.05	H1	91.7	218
	H2	103	246
	H3	111	264
	H4	124	294
	H5	129	308
	H6	142	339
0.00	I1	46.5	184
	I2	55.4	219
	I3	62.7	249
	I4	72.4	287
	I5	82.3	326
	I6	91.5	363

3-2.3 Self-Assembly and Scaling of the Lamellar Period

The isolated polymers were thermally annealed at 140℃ for 24 hours under modest pressure. Scanning electron microscope (SEM) images obtained for select block polymers with $N_{bb} \approx 200$ indicate long-range-ordered lamellar morphologies (Figure 3.5). Samples were also characterized by synchrotron-source small-angle X-ray scattering (SAXS). Raw 2D SAXS data are provided in Appendix B (Figure B.4). Representative azimuthally averaged SAXS profiles, corresponding to five samples with $z = 1$, are shown in Figure 3.6A. For all series, the scattering patterns are consistent with well-ordered lamellae.

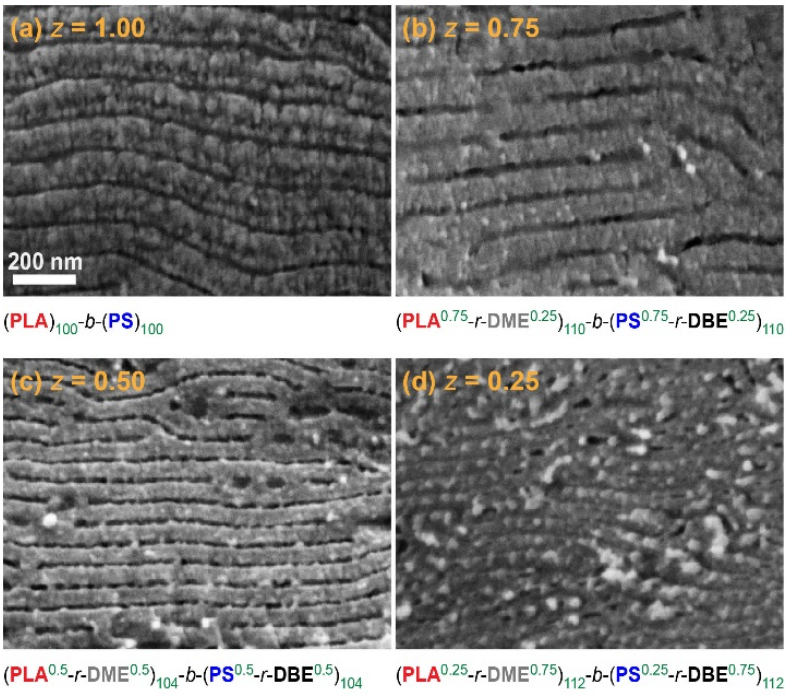

Figure 3.5: Scanning electron micrographs of graft block polymers with (*A*) $z = 1.00$, $(\mathbf{PLA})_{100}$-*b*-$(\mathbf{PS})_{100}$; (*B*) $z = 0.75$, $(\mathbf{PLA}^{0.75}$-*r*-$\mathbf{DME}^{0.25})_{110}$-*b*-$(\mathbf{PS}^{0.75}$-*r*-$\mathbf{DBE}^{0.25})_{110}$; (*C*) $z = 0.50$, $(\mathbf{PLA}^{0.5}$-*r*-$\mathbf{DME}^{0.5})_{104}$-*b*-$(\mathbf{PS}^{0.5}$-*r*-$\mathbf{DBE}^{0.5})_{104}$; and (*D*) $z = 0.25$, $(\mathbf{PLA}^{0.25}$-*r*-$\mathbf{DME}^{0.75})_{112}$-*b*-$(\mathbf{PS}^{0.25}$-*r*-$\mathbf{DBE}^{0.75})_{112}$.

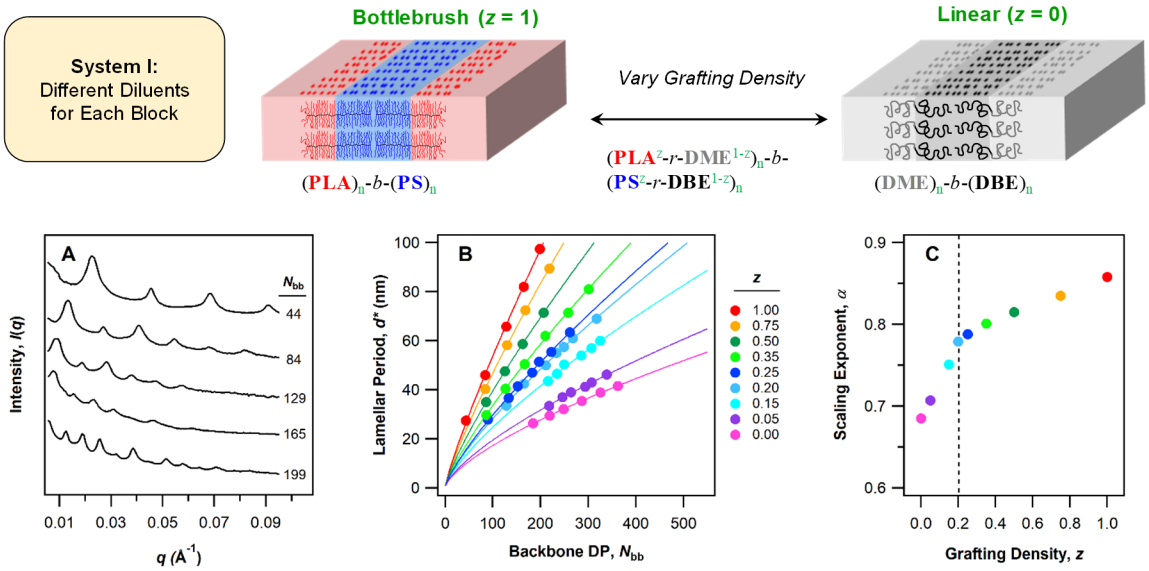

Figure 3.6: (*top*) Scheme of **System I**, comprising graft block polymers $(\mathbf{PLA}^{z}$-*r*-$\mathbf{DME}^{1-z})_n$-*b*-$(\mathbf{PS}^{z}$-*r*-$\mathbf{DBE}^{1-z})_n$ with variable total backbone degrees of polymerization ($N_{bb} = 2n$) and grafting densities (z). (*A*) Stacked 1D azimuthally averaged SAXS profiles for $z = 1$, indicating well-ordered lamellar morphologies. (*B*) Experimental data for the lamellar period (d^*) and N_{bb} (circles), as well as calculated power-law fits ($d^* \sim N_{bb}^{\alpha}$, lines). (*C*) Plot of the scaling exponents (α) as a function of z. A transition occurs around $z = 0.2$ (dotted line).

For all graft block polymers, the lamellar periods (d^*) were determined by indexing the raw SAXS data. Figure 3.6B shows plots of d^* *versus* N_{bb}. The scaling relationships for each series were calculated using a least-square power-law fitting function in *Igor*. To gain additional insight into the scaling behavior, the calculated scaling exponents α were plotted as a function of z (Figure 3.6C). For the $z = 1$ series, the large magnitude of α (0.86) is consistent with previously reported values for symmetric PLA-*b*-PS bottlebrush block polymers ($\alpha = 0.8–0.9$).[16-20,49] At the other extreme, the $z = 0$ series exhibits $\alpha = 0.69$, very close to the theoretical value ($\alpha = 2/3$) for strongly segregated symmetric linear diblock polymers.[7] The variable-z series ($z = 0.75$, 0.50, 0.35, 0.25, 0.20, 0.15, 0.05) constitute intermediate regimes bridging the two extremes. Comparing all series, the scaling exponents decrease monotonically with decreasing z. However, while α modestly decreases from 0.86 ($z = 1.00$) to 0.78 ($z = 0.20$), it then sharply decreases with decreasing z to 0.69 ($z = 0$). Collectively, these trends suggest changes in the backbone conformation with decreasing grafting density. Consistent with recent experimental and theoretical reports, at a certain critical z the conformational regime may transition from densely grafted brushes to loosely grafted brushes or combs.[50-51] These changes significantly impact the physical properties of graft homopolymers, such as the plateau modulus and extensibility. However, the effects of grafting density on block polymer phase behavior are unexplored to date. In Section 3-2.5, we will propose a model for the observed scaling behavior.

3-2.4 Synthesis and Self-Assembly: ***System II***

In this work, individual blocks can be treated as effectively homogeneous. No evidence of microphase separation is observed, even at low grafting densities and high total backbone degrees of polymerization [*e.g.*, each block (**PLA**$^{0.05}$-*r*-**DME**$^{0.95}$)$_{200}$ and (**PS**$^{0.05}$-*r*-**DBE**$^{0.95}$)$_{200,}$ Figure B.5]. To a first approximation, variations in χ between the backbone and side chains do not appear significant. However, varying the grafting density in **System I** may also affect the effective χ *between* blocks. Changing χ would influence d^* and potentially complicate the interpretations of the observed scaling trends. For symmetric linear diblock polymers, d^* exhibits a weak dependence on χ in the strongly segregated regime ($d^* \sim \chi^{1/6}$) and is independent of χ in the weakly segregated regime. In the mean-field Flory-Huggins lattice model, χ is determined by the number of nearest neighbor

contacts per monomer. In our materials, since the number ratio of diluents to side chain monomers (*i.e.*, either lactide or styrene repeats) is very small, the diluents are not expected to significantly affect χ. We anticipate that the large size disparity between macromonomers and diluents should make polymer architecture the primary factor responsible for the observed trends.

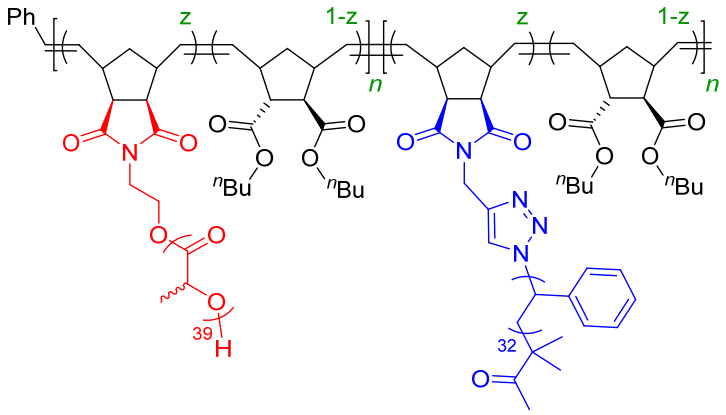

Scheme 3.3: (**PLA**^{z}-*r*-**DBE**$^{1-z}$)$_n$-*b*-(**PS**^{z}-*r*-**DBE**$^{1-z}$)$_n$ of variable backbone degrees of polymerization ($N_{bb} = 2n$ = 82–533) and grafting densities (z = 0.75, 0.50, 0.35, 0.25, 0.15, 0.12, 0.06, and 0.05).

To test this hypothesis, we synthesized **System II**, using the same diluent (**DBE**) to vary z in both blocks (Scheme 3.3). The lowest-z extreme (z = 0) in **System II** is the homopolymer (**DBE**)$_n$, which does not microphase separate. Macromonomers **PLA** (M_n = 3030 g/mol) and **PS** (M_n = 3800 g/mol) of similar molecular weights as those in **System I** were used. The determined reactivity ratios (r_{PLA} = 1.04, r_{DBE} = 0.89; r_{PS} = 0.83, r_{DBE} = 1.16) indicate random copolymerization within each block and therefore uniform grafting density. As for **System I**, polymers of general formula (**PLA**^{z}-*r*-**DBE**$^{1-z}$)$_n$-*b*-(**PS**^{z}-*r*-**DBE**$^{1-z}$)$_n$ were prepared ($N_{bb} = 2n$ = 82–533; z = 0.75, 0.50, 0.35, 0.25, 0.15, 0.12, 0.06, 0.05). The isolated monodisperse ($Đ$ = 1.02–1.19) copolymers were characterized by NMR and SEC. The compositions of all samples in **System II** are presented in Table 3.2.

Table 3.2: Total number-average molecular weights (M_n) and total backbone degrees of polymerization (N_{bb}) (**PLA**^{z}-*r*-**DBE**$^{1-z}$)$_n$-*b*-(**PS**^{z}-*r*-**DBE**$^{1-z}$)$_n$ graft block polymers (**System II**).

z	ID	M_n (kDa)	N_{bb}	z	ID	M_n (kDa)	N_{bb}
0.75	J1	116	44	0.15	N1	98.5	129
	J2	215	82		N2	161	212
	J3	330	125		N3	193	253
	J4	402	152		N4	213	279
	J5	521	198		N5	251	329
	J6	649	246		N6	299	392
0.50	K1	249	135	0.12	O1	150	224
	K2	322	174		O2	183	274
	K3	396	213		O3	221	330
	K4	472	254		O4	248	370
	K5	529	285		O5	274	409
	K6	603	325		O6	302	451
0.35	L1	241	174	0.06	P1	156	324
	L2	307	221		P2	177	367
	L3	364	263		P3	199	413
	L4	436	314		P4	226	469
	L5	472	341		P5	257	533
	L6	538	388	0.05	Q1	152	337
0.25	M1	232	216		Q2	169	376
	M2	277	258		Q3	184	408
	M3	335	312		Q4	203	451
	M4	384	358				
	M5	406	378				
	M6	472	439				

The samples were thermally annealed under the same conditions as **System I.** All of the polymers in **System II** self-assembled into well-ordered lamellae as evidenced by SAXS (Appendix B, Figure B.6). Azimuthally averaged 1D SAXS plots obtained for the z = 0.75 series are shown in Figure 3.7A as representative examples. Figure 3.7B shows the power-law fits (d^* vs. N_{bb}) for each series. The α values in **System II** are uniformly smaller compared to their counterparts of the same grafting density in **System I**. This observation could be attributed to the larger changes in χ between blocks upon decreasing z. The z = 0.05 series displays an α value of 0.52, approaching the theoretical value in the weak segregation limit (α = 1/2).[6-7] Comparing Figures 3.6C and 3.7C suggests that the different d^* and α values likely reflect changes in χ. The linear diblock polymer (**DME**)$_n$-*b*-(**DBE**)$_n$,

which is exactly the $z = 0$ series in **System I**, is itself strongly segregated, whereas the $z = 0$ series in **System II** is the homopolymer $(\mathbf{DBE})_n$. However, we note that the transition between regions of shallow and steep decreases in α with decreasing z occurs at nearly the same z in both systems ($z \approx 0.2$), suggesting that such transition is intrinsically related to polymer architecture rather than segregation strengths.

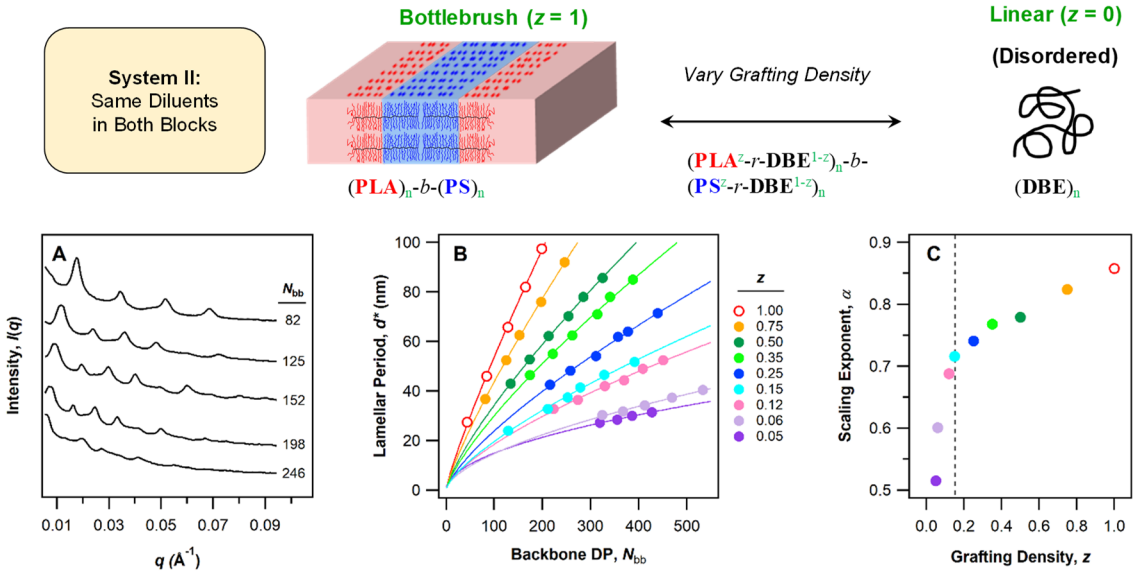

Figure 3.7: (*top*) Scheme of **System II**, comprising graft block polymers $(\mathbf{PLA}^{z}\text{-}r\text{-}\mathbf{DME}^{1-z})_n\text{-}b\text{-}(\mathbf{PS}^{z}\text{-}r\text{-}\mathbf{DBE}^{1-z})_n$ with variable total backbone degrees of polymerization ($N_{bb} = 2n$) and grafting densities (z). (*A*) Stacked 1D azimuthally averaged SAXS profiles for $z = 0.75$, indicating well-ordered lamellar morphologies. (*B*) Experimental data for the lamellar period (d^*) and N_{bb} (circles), as well as calculated power-law fits ($d^* \sim N_{bb}^{\alpha}$, lines). (*C*) Plot of the scaling exponents (α) as a function of z. A transition occurs around $z = 0.2$ (dotted line). Note that in (*B*) and (*C*), unfilled circles correspond to data for **System I** ($z = 1.00$), in which the side chain molecular weights are slightly higher.

We further highlight the significance of grafting density effects on the scaling of the lamellar period by predicting the required N_{bb} to reach an arbitrary value of $d^* = 200$ nm (Figure 3.8). Such a large d^* is desired for photonic applications. At the same z, N_{bb} required to reach $d^* = 200$ is larger for block polymers in **System II** than in **System I** as a result of differences in segregation strengths. In both systems, the predicted N_{bb} values exponentially increase with decreasing z below the observed transition ($z < 0.20$). In the linear block polymer limit ($z = 0$, **System I**), the required N to reach $d^* = 200$ nm is close to 4000. Such high-molecular-weight linear polymers are extremely challenging to

synthesize, and as a result there are very few examples of linear block polymers that can self-assemble to visible-light-reflecting photonic crystals.[52] Existing examples are typically limited by low conversion and inability to process the materials from the melt. In contrast, a 50% grafted block polymer should only require $N_{bb} \approx 730$. Manipulating the grafting density through copolymerization therefore constitutes a promising strategy to overcome limitations associated with both synthesis and processing. Further discussion of grafting density as a design parameter for polymer photonic crystals can be found in Chapter 6-2.2.

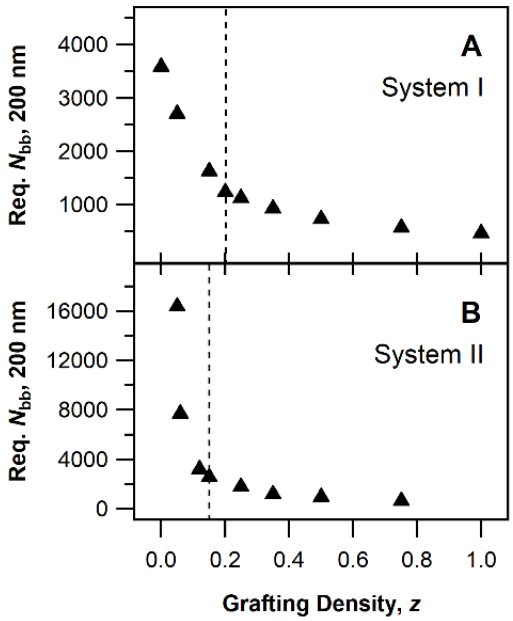

Figure 3.8: Plots of predicted N_{bb} required to access $d^* = 200$ nm as a function of grafting density (z) for (*A*) **System I** and (*B*) **System II**.

3-2.5 Interpretation of the Scaling Trends

We derive a potential model in order to relate the observed changes in α with grafting density (z) to the conformations of the graft polymer backbone and side chains. Key experimental results to capture include (1) the monotonic decrease in α with z (Figures 3.6C and 3.7C), (2) the apparent transition between shallow and steep decreases in α at a critical $z_c = 0.2$, and (3) potential segregation effects that emerge at low z. Comparison of two systems – one in which all series ($z \geq 0$) are in the strongly segregated limit (SSL)

(**System I**) and one that bridges the strongly and weakly segregated limits (WSL) (**System II**) – suggests that architecture effects, not segregation effects, are primarily responsible for the observed trends. We will begin by framing our results in the context of existing theory for the self-assembly of diblock polymers, then propose a functional form for the observed relationship between z and d^*, *i.e.*, $d^* \sim N_{bb}^{f(z)}$. We note that, in part due to the long-standing challenges associated with synthesizing well-defined graft polymers, there is not currently a theoretical or experimental consensus detailing the effects of grafting density on block polymer self-assembly.

The scaling of the lamellar period (d^*) is well-understood in the case of symmetric linear diblock polymers.[6-7,53] The magnitude of d^* is determined by the balance between the elastic energy ($F_{stretch}$), which resists chain stretching, and the interfacial energy (F_{int}), which resists expansion of block junctions along the domain interfaces. The stretching free energy per polymer chain is inversely proportional to the mean-square end-to-end distance, $\langle R^2 \rangle$:

$$\frac{F_{\text{stretch}}}{kT} \sim \frac{d^{*2}}{\langle R^2 \rangle} \qquad \text{Eq. 3-4}$$

When the chain is flexible, the mean-square end-to-end distance is given by $\langle R^2 \rangle = a_0^2 N_{bb}$, where a_0 is the statistical segment length and N_{bb} is the backbone degree of polymerization. (Note that in the case of linear polymers, N_{bb} is identical to the *total* degree of polymerization.) The interfacial energy per polymer chain is

$$\frac{F_{\text{int}}}{kT} \sim \gamma A \qquad \text{Eq. 3-5}$$

where γ is the surface tension and A is the area per chain. These parameters can be approximated by $\gamma = \chi^{\frac{1}{2}} a_0^{-2}$ and $A \sim N_{bb} {a_0}^3 / d^*$, leading to the following expression:

$$\frac{F_{\text{int}}}{kT} \sim \frac{N_{bb} a_0 \chi^{\frac{1}{2}}}{d^*} \qquad \text{Eq. 3-6}$$

In the SSL, the elastic energy and interfacial energy are balanced ($F_{stretch} = F_{int}$), and thus we obtain

$$d^* \sim \chi^{\frac{1}{6}} N^{\frac{1}{3}} [\langle R^2 \rangle]^{\frac{1}{3}} \sim a_0 \chi^{\frac{1}{6}} {N_{\mathrm{bb}}}^{\frac{2}{3}} \quad \text{Eq. 3-7}$$

In the WSL, the chains do not significantly stretch at the interface because χ is small, and thus F_{int} is effectively negligible. Therefore,

$$d^* \sim [\langle R^2 \rangle]^{\frac{1}{2}} \sim a_0 {N_{\mathrm{bb}}}^{\frac{1}{2}} \quad \text{Eq. 3-8}$$

Collectively, following Eqs. 3-7 and 3-8, the scaling relationship for diblock polymers has the general form

$$d^* \sim a_0 {N_{\mathrm{bb}}}^{\alpha} \quad \text{Eq. 3-9}$$

For flexible linear diblock polymers, typically $1/2 \leq \alpha \leq 2/3$. In contrast, when the polymer is semi-flexible, the same general form applies but the scaling exponent α is larger.[54-55] Bottlebrush diblock polymers typically exhibit α close to 0.9, reflecting the extended backbone conformations due to the sterically demanding architecture.[18-19,27] We note that, in the limit of extremely long backbones, when the persistence length and cross-sectional diameter are much shorter than the contour length of the brush, the chain should become flexible and α should approach 2/3.[20,56] In the current study however, the graft polymers exclusively reside in the regime in which the backbone persistence length (l_{p}) is not negligible compared to N_{bb}.

For non-flexible polymers, the mean-square end-to-end distance can be written as

$$\langle R^2 \rangle = a_0^2 C_\infty N_{\mathrm{bb}} \quad \text{Eq. 3-10}$$

by adopting Flory's characteristic ratio, $C_\infty = 2l_{\mathrm{p}}/a_0$. Therefore,

$$\langle R^2 \rangle = 2a_0 l_{\mathrm{p}} N_{\mathrm{bb}} \quad \text{Eq. 3-11}$$

For bottlebrush polymers, l_{p} is a function of the side chain degree of polymerization (N_{sc}) and z.[51,57] l_{p} is also anticipated to be a function of N_{bb} by theory and simulations,[50,58] but the functional form of this relationship is currently a matter of some debate. We will assume that C_∞ is a function of N_{bb} and z in order to study how the backbone stiffness affects d^*.

Two boundary conditions of this function are known. First, when $z = 0$, $C_\infty = 1$ by definition since the backbone is identical to a flexible linear polymer. Second, in the

opposite limit, when $z = 1$, C_∞ should approach N_{bb}. To satisfy these conditions, we write the following power function describing the relationship between C_∞ and N_{bb}:

$$C_\infty = {N_{bb}}^{mz+b} \quad \text{Eq. 3-12}$$

We now insert Eq. 3-12 into Eq. 3-10, then rewrite the expressions for d^* in the SSL (Eq. 3-7) and WSL (Eq. 3-8) in terms of C_∞:

$$d^* \sim \begin{cases} a_0 \chi^{\frac{1}{6}} {C_\infty}^{\frac{1}{3}} {N_{bb}}^{\frac{2}{3}} & \text{SSL} \\ a_0 {C_\infty}^{\frac{1}{2}} {N_{bb}}^{\frac{1}{2}} & \text{WSL} \end{cases} \quad \text{Eq. 3-13}$$

Therefore, the experimentally observed scaling exponents α can be written as follows:

$$\alpha = \begin{cases} \dfrac{mz+b+2}{3} & \text{SSL} \\ \dfrac{mz+b+1}{2} & \text{WSL} \end{cases} \quad \text{Eq. 3-14}$$

We now apply Eq. 14 to **Systems I** and **II** in order to evaluate how C_∞, as a proxy for the backbone stiffness, changes with z. In **System I**, different diluents (**DME** and **DBE**) are used to vary z in each block. The linear diblock polymer **DME**-*b*-**DBE** exhibits $\alpha = 0.69 \approx 2/3$. This result suggests that, even in the $z = 0$ limit, the block polymers in **System I** are strongly segregated. Since α should only increase with z, all series in **System I** are expected to be in the SSL. Figure 3.9A shows the lines of best fit for experimentally determined values of α and z. Two regions were identified, diverging at a critical grafting density $z_{c,I}$: (1) when $z < 0.2$, α steeply decreases with decreasing z; (2) when $z > 0.2$, α slightly decreases with decreasing z. In the first region, $\alpha = 0.46z + 0.68$; in the second region, $\alpha = 0.091z + 0.77$. The lines of best fit intersect at $z_{c,I} = 0.23$. We obtain the following expressions for C_∞:

$$C_\infty = \begin{cases} {N_{bb}}^{1.39z} & z < 0.23 \\ {N_{bb}}^{0.27z+0.30} & z > 0.23 \end{cases} \quad \text{Eq. 3-15}$$

Introducing Eq. 3-15 into Eq. 3-10 enables calculations of the normalized root-mean-square end-to-end distances ($\sqrt{\langle R^2 \rangle}/a_0$) as a function of z (Figure 3.9A). The transition in $\sqrt{\langle R^2 \rangle}/a_0$ occurs near $z_{c,I}$: $z = 0.27$.

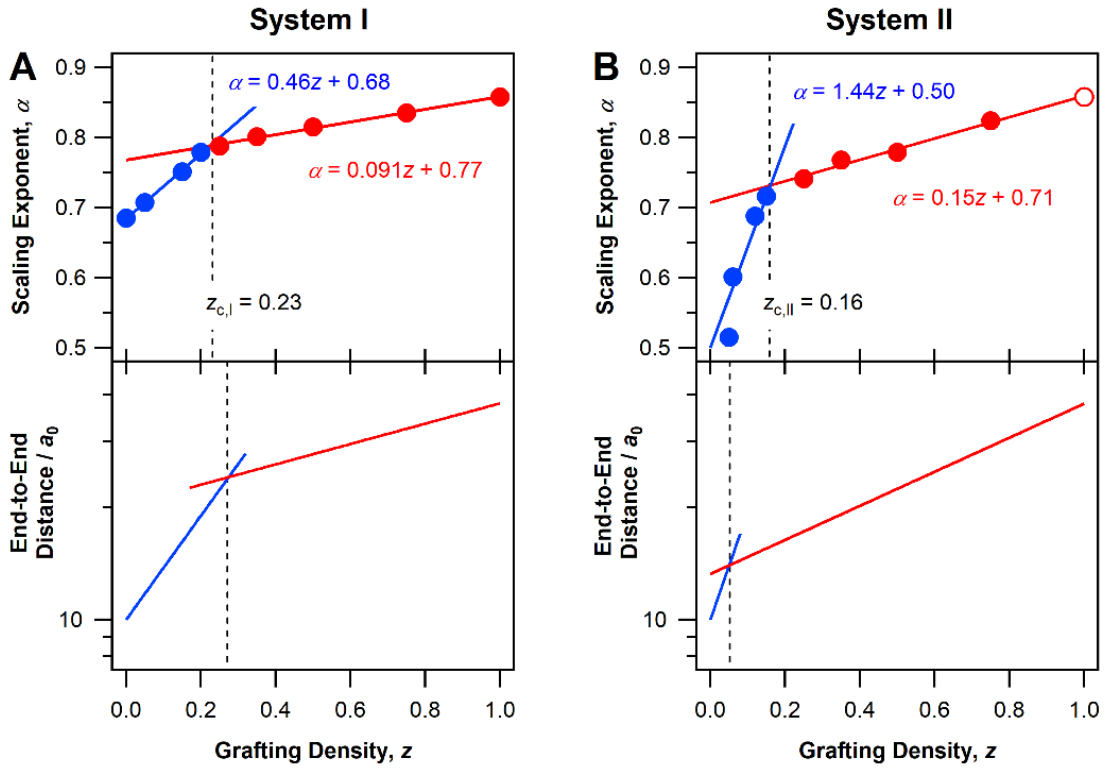

Figure 3.9: Analysis of scaling trends with grafting density (z) for (*A*) **System I** and (*B*) **System II**. (*top*) Experimentally determined values and lines of best fit for the scaling exponent (α) *versus* z. The lines intersect at a critical z_c, associated with a transition in the backbone stiffness. In (b), the unfilled circle (z = 1.00) indicates data for **System I**. (*bottom*) Calculated root-mean-square end-to-end distances, normalized by the backbone statistical segment length ($\sqrt{\langle R^2 \rangle}/a_0$), fixing N_{bb} = 100.

Unlike **System I**, **System II** uses the same diluent (**DBE**) for both blocks. The z = 0 limit constitutes a linear homopolymer rather than a diblock polymer, and therefore the segregation behavior and chain stretching at the domain interface differ between **Systems I** and **II**. Applying the same analysis for **System II**, when the grafting density is low (z < 0.2) we obtain $\alpha = 1.44z + 0.50$ (Figure 3.9B). In this region, the block polymers experience intermediate to weak segregation (α < 2/3). Reflecting the boundary condition C_∞ = 1 at z = 0, the y-intercept was fixed at 1/2. Therefore, applying Eq. 3-14 in the WSL, m = 2.87 and b = 0. By comparison to **System I** and literature results, we expect the series to experience strong segregation at a certain z. We will assume that, at least when z > 0.2, the block polymers are in the SSL. Therefore, $\alpha = 0.15z + 0.71$ suggests m = 0.46, b = 0.12.

The lines of best fit intersect at $z_{c,II} = 0.16$. From these results, for **System II** we obtain the following expression for C_∞:

$$C_\infty = \begin{cases} {N_{bb}}^{2.87z} & z < 0.16 \\ {N_{bb}}^{0.46z+0.12} & z > 0.16 \end{cases} \quad \text{Eq. 3-16}$$

Figure 3.9B (*bottom*) shows the values of $\sqrt{\langle R^2 \rangle}/a_0$ calculated for **System II** per Eq. 3-16. Surprisingly, $\sqrt{\langle R^2 \rangle}/a_0$ exhibits an apparent transition at $z = 0.05$, much lower than the value $z_{c,II} = 0.16$ identified by fitting the experimental data (Figure 3.9B, *top*). In contrast, for **System I** the transitions in α and $\sqrt{\langle R^2 \rangle}/a_0$ occur at approximately the same z (Figure 3.9A). Since $\sqrt{\langle R^2 \rangle}/a_0$ is obtained from fitting α in two regions (diverging at a critical z_c and assuming either weak or strong segregation), the transitions should occur at the same z if the proposed model accurately describes the entire z range. The observed mismatch suggests that our model does not reflect all factors affecting d^* in the transition region. The preceding discussions have focused on the backbone stiffness. However, the potential contributions of χ and side chain conformations should also be considered.

Figure 3.9 indicates that changes in C_∞ alone do not fully capture the scaling of the lamellar period. Changes in the segregation strength that emerge with decreasing z are likely also significant. In **System I**, the diluents are different and the polymers are already stretched at $z = 0$ (inferred based on $\alpha > 2/3$). Since the backbones are already stretched, increasing z may not significantly affect χ between the two grafted blocks or backbone stretching. A high grafting density (large z_c) may be required to further stretch the chains. In **System II** however, the $z = 0$ limit describes linear homopolymers, which are expected to adopt unperturbed conformations. Therefore, the onset of backbone and side chain stretching should occur at a lower z_c. The effects of segregation, as well as the precise location of the transition between SSL and WSL with z, are important factors to consider.

To conclude our interpretation of the scaling relationships, we address the potential role of the side chains in the experimentally observed transition at $z_c \approx 0.20$. Our analysis is consistent with C_∞ changing abruptly at z_c. We note that, for **System I**, all series ($0 \leq z \leq 1$) are in the SSL. Steric repulsion between the side chains is expected to be the primary

factor responsible for increasing C_∞. The location of the transition z_c is therefore expected to be related to the onset of side chain overlap. The radius of gyration of a side chain is

$$R_{g,sc} = a_{sc}\,(N_{sc}/6)^{\frac{1}{2}} \qquad \text{Eq. 3-17}$$

where a_{sc} is the statistical segment length of the side chain. In order for the side chains to retain their unperturbed conformations, the contour length of a section of backbone separating adjacent side chains (L_g) should be larger than the side chain diameter, $d_{sc} = 2R_{g,sc}$. As z increases, the side chains are expected to stretch to accommodate tethering at shorter L_g.[57] Consistent with a convention employed by previous theories and experiments for bottlebrush polymers,[20] we assume that the contour length per polynorbornene backbone segment is constant (L_s = 0.62 nm). The number of backbone segments between adjacent grafting points (inclusive) is provided by $1/z$, and L_g follows:

$$L_g = \frac{L_s}{z} \qquad \text{Eq. 3-18}$$

When $L_g > d_{sc}$, the backbone is expected to behave as a flexible Gaussian chain. When $L_g < d_{g,sc}$, the backbone is expected to stretch, ultimately leading to wormlike chain conformations at sufficiently high z. The stiffness of the brush is expected to increase when two neighboring grafts contact each other in the limiting range of the torsional angle. We define z_s as the grafting density at the onset of backbone stretching due to torsional limitations ($L_g = d_{sc}$):

$$z_s \equiv \frac{L_s}{2a_{sc}\,(N_{sc}/6)^{\frac{1}{2}}} \qquad \text{Eq. 3-19}$$

As an approximation, we estimate that the transition in the brush conformation responsible for the transition in α occurs when $z = z_s$. We note that stretching of the side chains at $z > z_s$ may not permit this simple approximation, since stretching of the graft polymer backbone and side chains should compete to balance conformational entropy. We further assume N_{sc} = 36 and $L_s \approx a_{sc}$, producing z_s = 0.20. For both **Systems I** and **II**, the experimentally observed transition in α occurs at $z_c \approx z_s$ ($z_{c,I}$ = 0.23, $z_{c,II}$ = 0.16). This observation suggests that the steep increase in α at small z is mainly due to the stretching of the backbone,

whereas the modest increase in α at high z is mainly due to the increasing torsional angle demanded by decreasing L_g.

These results collectively suggest that changes in the end-to-end distance $\langle R^2 \rangle$ are primarily responsible for the increase in α with increasing z. $\langle R^2 \rangle$ may increase due to a combination of backbone stretching, torsional limitations, and χ effects. $\langle R^2 \rangle$ exhibits two regimes in terms of z dependence, potentially corresponding to a transition between loose and densely grafted brushes.[50-51] In our model, we propose functional forms for (1) the relationship between backbone stiffness and backbone length ($C_\infty \sim N_{bb}^{f(z)}$) and (2) the relationship between the lamellar period scaling exponent and grafting density ($\alpha \sim mz + b$). We anticipate that the materials and framework outlined herein should stimulate additional theories and experiments.

The self-assembly of block polymers enables diverse practical applications. We herein provide experimental evidence that quantitatively correlates grafting density with scaling of the lamellar period. Through the analyses of well-defined graft block polymer assemblies, we show that the scaling exponent undergoes a sharp transition at $z \approx 0.20$. The observed transition is attributed to different conformational regimes dictated by backbone chain conformations. We expect that the determined scaling relationships for various grafting density series could be exploited to guide material design.

3-3 Impact of Grafting Density on Linear Rheology

The preceding sections have demonstrated the impact of varying the molecular architecture on *static* properties, such as the scaling of the block polymer lamellar period. This section will provide insight into the *dynamic* consequences.

Graft polymers bearing poly(D,L-lactide) side chains were synthesized by living ring-opening metathesis copolymerization (Chapter 2). The grafting density (z) was varied across the linear, comb, and bottlebrush regimes ($0 \leq z \leq 1$), and for each z, the side chain molecular weight (N_{sc}) was fixed while the total backbone degree of polymerization (N_{bb}) was varied. The linear rheology of these (**PLA**^{z}-*r*-**DME**$^{1-z}$)$_n$ graft polymers was studied as a function of z and N_{bb} by our collaborators at the University of Minnesota (Ingrid Haugan Smidt, Dr.

Michael Maher, Prof. Marc Hillmyer, and Prof. Frank Bates). This section will present our contributions to the synthesis and molecular characterization, then summarize key insights into the chain conformation. We will discuss the impact of grafting density in the context of linear rheology, but since the measurements and analysis were performed by our collaborators, we defer further discussion to the published reference.[59]

Graft polymers have inspired significant interest due to their unique properties (*e.g.*, high entanglement molecular weight[50,60-62] and low viscosity[39,63-64]) and diverse applications. Recent theoretical and experimental efforts have focused on translating the dynamics of *linear* polymers into models to predict the physical properties of *graft* polymers. However, the underlying dynamics of graft architectures remain relatively unexplored. Due to long-standing synthetic challenges, theoretical efforts to develop a universal model of graft polymer dynamics[22,50-51,65-67] have outpaced experimental studies.

We recently developed a ring-opening metathesis copolymerization strategy that enables precise control over z, N_{sc}, and N_{bb} (Chapter 2). Eight series of (**PLA**^{z}-*r*-**DME**$^{1-z}$)$_n$ graft polymers (z = 1.00, 0.50, 0.40, 0.25, 0.20, 0.15, 0.05, 0) were synthesized by copolymerizing an ω-norbornenyl **PLA** macromonomer ($M_{n,PLA}$ = 3450 g/mol) with a discrete norbornenyl dimethyl ester diluent, **DME**. We note that the side chains do not entangle since $M_{n,PLA} < M_{e,PLA}$, the entanglement molecular weight of poly(D,L-lactide). Grafting-through ROMP guarantees fixed N_{sc} and permits varying N_{bb} while maintaining low dispersity ($Đ < 1.2$). **Table 3.3** summarizes the molecular characterization data. SEC traces are provided in Appendix B (Figure B.7).

The impact of grafting density on the viscoelastic behavior was systematically studied by dynamic mechanical analysis. Dynamic master curves were created by time–temperature superposition (TTS) of the data relative to the reference temperature $T_{ref} = T_g$ + 34 °C. The thermorheological simplicity of all samples was validated in four ways: (1) the appearance of only one glass transition temperature (T_g) as determined by differential scanning calorimetry; (2) no microphase separation between the grafts and backbone based on SAXS; (3) ability to fit all data to the Williams–Landel–Ferry (WLF) model with a single set;[68] and (4) continuity in van Gurp-Palmen plots.[69]

Table 3.3: Molecular and thermal characterization data for (**PLA**^{z}-*r*-**DME**$^{1-z}$)$_n$ graft polymers.

Sample ID	z	M_w (kg/mol)	N_{bb}[a]	$Đ$	T_g (°C)	η_0 (10^3 Pa·s)
$(PLA)_{12}$	1.00	40.3	12	1.04	54	6.1
$(PLA)_{24}$	1.00	81.6	24	1.01	53	12
$(PLA)_{55}$	1.00	189	55	1.01	52	18
$(PLA)_{97}$	1.00	335	97	1.03	52	39
$(PLA)_{200}$	1.00	676	200	1.03	52	94
$(PLA)_{510}$	1.00	1770	510	1.05	53	270
$(PLA)_{1100}$	1.00	3960	1100	1.10	54	540
$(PLA)_{2900}$	1.00	10000	2900	1.37	51	30000
$(PLA^{0.5}$-*r*-$DME^{0.5})_{22}$	0.50	40.7	22	1.04	53	9.0
$(PLA^{0.5}$-*r*-$DME^{0.5})_{85}$	0.50	156	85	1.02	52	22
$(PLA^{0.5}$-*r*-$DME^{0.5})_{460}$	0.50	840	460	1.04	53	170
$(PLA^{0.5}$-*r*-$DME^{0.5})_{960}$	0.50	1760	960	1.06	54	620
$(PLA^{0.5}$-*r*-$DME^{0.5})_{2600}$	0.50	4840	2600	1.13	53	4600
$(PLA^{0.4}$-*r*-$DME^{0.6})_{440}$	0.40	658	440	1.04	52	–
$(PLA^{0.4}$-*r*-$DME^{0.6})_{1600}$	0.40	2440	1600	1.11	51	–
$(PLA^{0.25}$-*r*-$DME^{0.75})_{40}$	0.25	41.2	40	1.04	53	7.3
$(PLA^{0.25}$-*r*-$DME^{0.75})_{62}$	0.25	63.2	62	1.02	52	17
$(PLA^{0.25}$-*r*-$DME^{0.75})_{88}$	0.25	90.0	88	1.01	54	16
$(PLA^{0.25}$-*r*-$DME^{0.75})_{130}$	0.25	133	130	1.02	53	33
$(PLA^{0.25}$-*r*-$DME^{0.75})_{210}$	0.25	217	210	1.01	53	55
$(PLA^{0.25}$-*r*-$DME^{0.75})_{270}$	0.25	276	270	1.02	53	100
$(PLA^{0.25}$-*r*-$DME^{0.75})_{330}$	0.25	341	330	1.02	53	120
$(PLA^{0.25}$-*r*-$DME^{0.75})_{410}$	0.25	417	410	1.02	53	190
$(PLA^{0.25}$-*r*-$DME^{0.75})_{640}$	0.25	650	640	1.03	54	450
$(PLA^{0.25}$-*r*-$DME^{0.75})_{840}$	0.25	855	840	1.03	53	880
$(PLA^{0.25}$-*r*-$DME^{0.75})_{1500}$	0.25	1480	1500	1.07	54	5100
$(PLA^{0.25}$-*r*-$DME^{0.75})_{1800}$	0.25	1850	1800	1.11	53	12000
$(PLA^{0.2}$-*r*-$DME^{0.8})_{120}$	0.20	103	120	1.02	52	–
$(PLA^{0.2}$-*r*-$DME^{0.8})_{1100}$	0.20	905	1100	1.04	53	–
$(PLA^{0.15}$-*r*-$DME^{0.85})_{88}$	0.15	60.9	88	1.02	55	25
$(PLA^{0.15}$-*r*-$DME^{0.85})_{170}$	0.15	116	170	1.01	56	100
$(PLA^{0.15}$-*r*-$DME^{0.85})_{420}$	0.15	292	420	1.02	55	1600
$(PLA^{0.15}$-*r*-$DME^{0.85})_{720}$	0.15	501	720	1.03	56	12000
$(PLA^{0.15}$-*r*-$DME^{0.85})_{1500}$	0.15	1010	1500	1.04	53	200000
$(PLA^{0.05}$-*r*-$DME^{0.95})_{200}$	0.05	76.1	200	1.01	59	130
$(PLA^{0.05}$-*r*-$DME^{0.95})_{410}$	0.05	154	410	1.01	59	1200
$(PLA^{0.05}$-*r*-$DME^{0.95})_{950}$	0.05	352	950	1.02	59	14000
$(DME)_{100}$	0	20.1	100	1.01	83	8.1
$(DME)_{200}$	0	41.2	200	1.01	89	55
$(DME)_{510}$	0	107	510	1.01	88	200
$(DME)_{900}$	0	188	900	1.01	89	11000

[a] Weight-average total backbone degree of polymerization.

The zero-shear viscosities were obtained from the terminal regimes of the dynamic master curves ($\eta_0 = G''/\omega$) and plotted as a function of the weight-average total molecular weight, M_w (Figure 3.10). The data in Figure 3.10 can be fit using $\eta_0 \sim M_w^{\beta}$ with β = either 1 or 3, consistent with Rouse or reptation scaling, respectively. For the z = 0.25 series, an abrupt transition in β is observed ($M_w \approx 600$ kg/mol), suggesting that these graft polymers follow the same fundamental relaxation processes as linear polymers. The increased viscosities of the highest-molecular-weight samples in the z = 0.50 and z = 1.0 series are also consistent with a transition from Rouse to reptation scaling. These results demonstrate that at a fixed total M_w, η_0 can be tuned over several orders of magnitude by adjusting the grafting density.

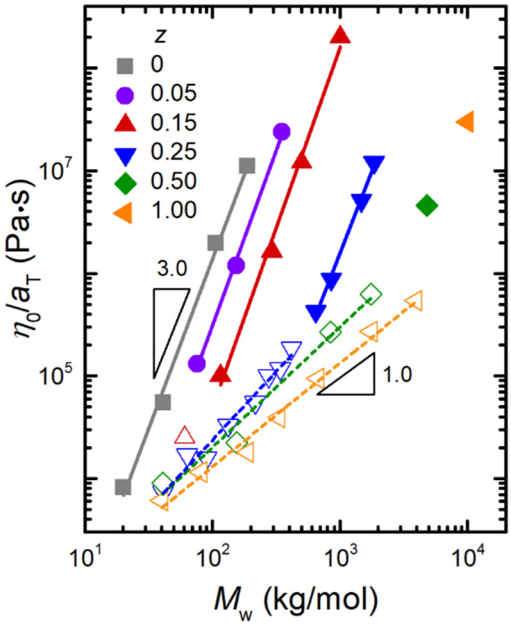

Figure 3.10: Reduced zero-shear viscosity (η_0 / a_T) versus M_w for six series with varying grafting density, z. Unentangled and entangled polymers are shown with open and filled symbols, respectively. Power-law fits are shown corresponding to Rouse (*dotted line*) or reptation (*solid line*) scaling.

For the series of graft polymers discussed in this chapter, the plateau modulus (G_e) was estimated from van Gurp-Palmen plots of the highest-M_w sample for each z (Appendix B, Figure B.8):

$$M_e = \frac{\rho RT}{G_e} \qquad \text{Eq. 3-20}$$

where the melt density ρ = 1.25 g/cm^3 and $T = T_{ref}$. Daniel and coworkers have recently developed scaling laws based on theory to predict how G_e varies as a function of N_{sc} and the volume-normalized inverse grafting density ($n_g = z^{-1}$). (See also the discussion in Chapter 1.) As the scaling of G_e normalized by the plateau modulus of the analogous linear melt (= G_e / $G_{e,lin}$) varies, four distinct conformational regimes are predicted to emerge: (1) loose combs (LC), dense combs (DC), loose brushes (LB) and dense brushes (DB) (Figure 3.11A).[50] In comparison, our experimental data features a sharp transition from the DB regime (G_e / $G_{e,lin} \sim n_g^{1.2}$) at high z to the LC regime at low z (Figure 3.11B). Contrary to predictions from theory, the DC and LB regimes are not observed.

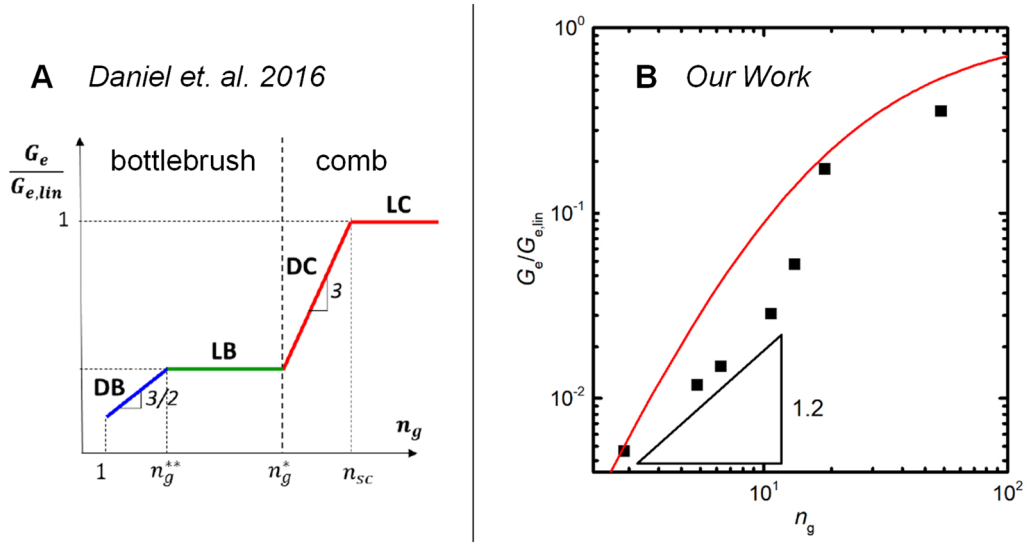

Figure 3.11. Dependence of the plateau modulus of graft polymer melts normalized by the plateau modulus of the analogous linear melt (G_e / $G_{e,lin}$) on the average backbone length between grafts (n_g). Different conformational regimes are identified as a function of n_g at constant N_{sc}. (*A*) Regimes predicted by Daniel et al. based on theory.[50] Adapted with permission from Nature Publishing Group. (*B*) Experimental data for (**PLA**^{z}-*r*-**DME**$^{1-z}$)$_n$ graft polymers.

Comparison of our experimental data and the existing theory exposes differences between real polymers and idealized model systems. For example, the theory assumes that $l_K >> n_g$ in all four scaling regimes, where l_K is the Kuhn length of the backbone. In practice however, n_g approaches l_K prior to reaching the dense brush limit. In addition, the side chains are assumed to pervade a configurational volume significantly larger than the actual space occupied by the side chain. However, the real side chains in our case are relatively short (N_{sc} = 45). As a consequence, the transition from barely overlapping to overly crowded side chains occurs across a rather narrow range of n_g, effectively bypassing the LB regime.

Increasing the length of the side chains would help reconcile this disparity between experiment and theory, but such changes may lead to side chain entanglement, complicating backbone relaxation.[33,70-75] Side chain entanglement would also negate the advantages of reduced modulus associated with the dense brush limit, forfeiting any supersoft quality imparted on the material by the architecture. The practical reality of these physical phenomena obscures the predictions of the theory in the ideal limit.

We propose an alternative model to predict the onset of entanglements in graft polymers. The model will be outlined herein to invite comparisons to the static consequences of graft polymer architecture discussed in Sections 3-1 and 3-2; additional discussion can be found in the published reference.[59] Relevant parameters include the side chain diameter ($d_{sc} = 2R_{g,sc}$) and the average backbone length between grafts (L_g), defined according to Eqs. 3-17 and 3-19, respectively (Section 3-3). Figure 3.12A shows the expected scaling of d_{sc} and $L_{g,sc}$ in the LC regime.

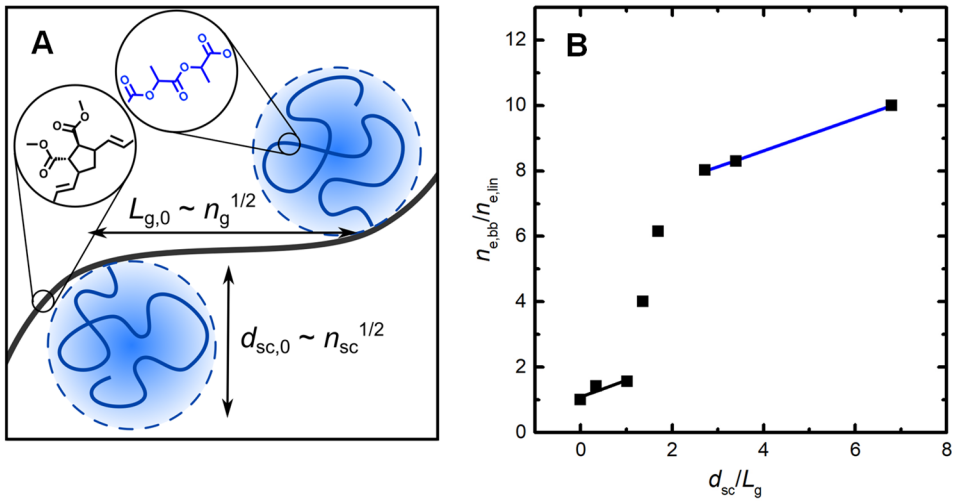

Figure 3.12: (*A*) Illustration of a comb polymer at low grafting density, in which the backbone and side chain are both unperturbed Gaussian coils. The unperturbed backbone length between grafts, $L_{g,0}$, and side chain diameter, d_{sc}, are indicated. (*B*) Entanglement data plotted as $N_{e,bb} / N_{e,lin}$ versus d_{sc} / L_g. The black and blue lines correspond to the low- and high-z limits, respectively. When $d_{sc} / L_g > 1$, steric repulsion between the side chains reduces the density of entanglements.

Figure 3.12B expresses the linear rheology data in terms of the backbone degree of polymerization between entanglements ($N_{e,bb}$) normalized by the degree of polymerization between entanglements of the corresponding linear melt ($N_{e,lin}$). Plotting $N_{e,bb} / N_{e,lin}$ versus

d_{sc} / L_g emphasizes the limiting behavior in the brush ($d_{sc} / L_g > 1$) and comb ($d_{sc} / L_g < 1$) limits. A sharp transition occurs when the side chains begin to overlap ($d_{sc} / L_g \approx 1$), corresponding to $z \approx 0.20$ in the studied system.

We note that a sharp transition near $z = 0.20$ is also observed in the scaling of the block polymer lamellar period, Section 3-3. The block polymers have effectively the same d_{sc} values as the PLA graft homopolymers studied by rheology, enabling direct comparison. Figure 3.13 plots the scaling exponents (α) for **System I** (Figure 3.9A) and the $N_{e,bb} / N_{e,lin}$ values for PLA graft homopolymers (Figure 3.12B) versus z. Remarkably, although the relevant physical phenomena are very different, both sets of data feature a sharp transition near $z = 0.20$. This result suggests potential deep connections between conformational changes with grafting density and physical properties. Future work will further explore these connections through complementary simulation and scattering studies. Improving understanding will enable progress toward a universal model for graft polymer conformation and properties.

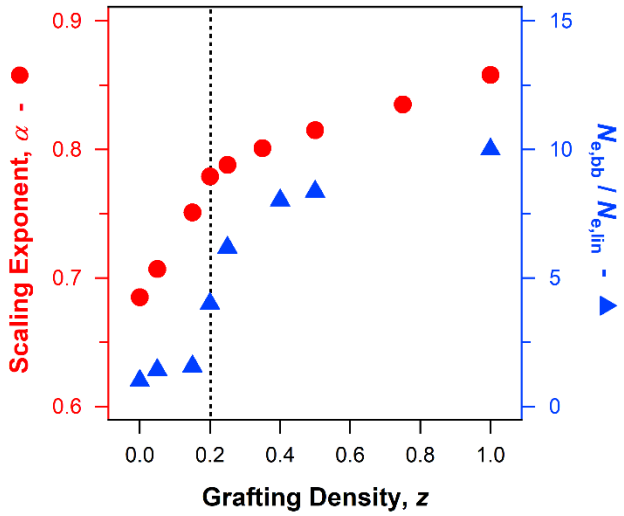

Figure 3.13: Direct comparison of the static and dynamic consequences of grafting density, z. (*left axis, red*) Scaling exponent α describing the change in the block polymer lamellar period with total backbone degree of polymerization ($d^* \sim N_{bb}^{\alpha}$). (*right axis, blue*) Normalized backbone degree of polymerization between entanglements ($N_{e,bb} / N_{e,lin}$).

In conclusion, the linear viscoelastic responses of eight sets of polymers with variable grafting densities were studied. At high grafting density, the polymers behave as dense

brushes (DB), where $G_e \sim n_g^{1.2}$ in good agreement with existing theory. Reducing the grafting density results in a sharp transition to the loose comb (LC) regime. We propose a simple criterion for anticipating the onset of entanglement dynamics in graft polymers based on d_{sc} / L_g, the ratio of the diameter of gyration of the side chains to the average backbone contour length between grafts. When $d_{sc}/L_g < 1$ the polymers behave as thin flexible chains with conformations dictated by the backbone chemistry, while $d_{sc}/L_g > 1$ leads to thick semiflexible cylinders and a chain configuration governed by the molecular architecture.

3-4 References

(1) Pesek, S. L.; Li, X.; Hammouda, B.; Hong, K.; Verduzco, R. *Macromolecules* **2013**, *46*, 6998–7005.
(2) Pesek, S. L.; Xiang, Q.; Hammouda, B.; Verduzco, R. *J. Polym. Sci., Part B: Polym. Phys.* **2017**, *55*, 104–111.
(3) Kikuchi, M.; Nakano, R.; Jinbo, Y.; Saito, Y.; Ohno, S.; Togashi, D.; Enomoto, K.; Narumi, A.; Haba, O.; Kawaguchi, S. *Macromolecules* **2015**, *48*, 5878–5886.
(4) Gerle, M.; Fischer, K.; Roos, S.; Müller, A. H. E.; Schmidt, M.; Sheiko, S. S.; Prokhorova, S.; Möller, M. *Macromolecules* **1999**, *32*, 2629–2637.
(5) Sing, C. E.; Zwanikken, J. W.; Cruz, M. O. d. l. *J. Chem. Phys.* **2015**, *142*, 034902.
(6) Matsen, M. W.; Bates, F. S. *Macromolecules* **1996**, *29*, 1091–1098.
(7) Semenov, A. V. *Sov. Phys.-JETP (Engl. Transl.)* **1985**, *61*, 733–742.
(8) Hadjichristidis, N.; Pitsikalis, M.; Iatrou, H.; Pispas, S. *Macromol. Rapid Commun.* **2003**, *24*, 979–1013.
(9) Sheiko, S. S.; Sumerlin, B. S.; Matyjaszewski, K. *Prog. Polym. Sci.* **2008**, *33*, 759–785.
(10) Peng, S.; Bhushan, B. *RSC Adv.* **2012**, *2*, 8557–8578.
(11) Rzayev, J. *ACS Macro Lett.* **2012**, *1*, 1146–1149.
(12) Müllner, M.; Müller, A. H. E. *Polymer* **2016**, *98*, 389–401.
(13) Yavitt, B. M.; Gai, Y.; Song, D.-P.; Winter, H. H.; Watkins, J. J. *Macromolecules* **2017**, *50*, 396–405.
(14) Verduzco, R.; Li, X.; Pesek, S. L.; Stein, G. E. *Chem. Soc. Rev.* **2015**, *44*, 2405–2420.
(15) Vatankhah-Varnosfaderani, M.; Daniel, W. F. M.; Everhart, M. H.; Pandya, A. A.; Liang, H.; Matyjaszewski, K.; Dobrynin, A. V.; Sheiko, S. S. *Nature* **2017**, *549*, 497–501.
(16) Xia, Y.; Olsen, B. D.; Kornfield, J. A.; Grubbs, R. H. *J. Am. Chem. Soc.* **2009**, *131*, 18525–18532.
(17) Rzayev, J. *Macromolecules* **2009**, *42*, 2135–2141.
(18) Gu, W.; Huh, J.; Hong, S. W.; Sveinbjornsson, B. R.; Park, C.; Grubbs, R. H.; Russell, T. P. *ACS Nano* **2013**, *7*, 2551–2558.
(19) Sveinbjörnsson, B. R.; Weitekamp, R. A.; Miyake, G. M.; Xia, Y.; Atwater, H. A.; Grubbs, R. H. *Proc. Natl. Acad. Sci. U.S.A.* **2012**, *109*, 14332–14336.

(20) Dalsin, S. J.; Rions-Maehren, T. G.; Beam, M. D.; Bates, F. S.; Hillmyer, M. A.; Matsen, M. W. *ACS Nano* **2015**, *9*, 12233–12245.
(21) Lecommandoux, S.; Chécot, F.; Borsali, R.; Schappacher, M.; Deffieux, A.; Brûlet, A.; Cotton, J. P. *Macromolecules* **2002**, *35*, 8878–8881.
(22) Cao, Z.; Carrillo, J.-M. Y.; Sheiko, S. S.; Dobrynin, A. V. *Macromolecules* **2015**, *48*, 5006–5015.
(23) Zhang, B.; Gröhn, F.; Pedersen, J. S.; Fischer, K.; Schmidt, M. *Macromolecules* **2006**, *39*, 8440–8450.
(24) Miyake, G. M.; Piunova, V. A.; Weitekamp, R. A.; Grubbs, R. H. *Angew. Chem., Int. Ed.* **2012**, *51*, 11246–11248.
(25) Miyake, G. M.; Weitekamp, R. A.; Piunova, V. A.; Grubbs, R. H. *J. Am. Chem. Soc.* **2012**, *134*, 14249–14254.
(26) Piunova, V. A.; Miyake, G. M.; Daeffler, C. S.; Weitekamp, R. A.; Grubbs, R. H. *J. Am. Chem. Soc.* **2013**, *135*, 15609–15616.
(27) Macfarlane, R. J.; Kim, B.; Lee, B.; Weitekamp, R. A.; Bates, C. M.; Lee, S. F.; Chang, A. B.; Delaney, K. T.; Fredrickson, G. H.; Atwater, H. A.; Grubbs, R. H. *J. Am. Chem. Soc.* **2014**, 17374–17377.
(28) Sun, G.; Cho, S.; Clark, C.; Verkhoturov, S. V.; Eller, M. J.; Li, A.; Pavía-Jiménez, A.; Schweikert, E. A.; Thackeray, J. W.; Trefonas, P.; Wooley, K. L. *J. Am. Chem. Soc.* **2013**, *135*, 4203–4206.
(29) Kawamoto, K.; Zhong, M.; Gadelrab, K. R.; Cheng, L.-C.; Ross, C. A.; Alexander-Katz, A.; Johnson, J. A. *J. Am. Chem. Soc.* **2016**, *138*, 11501–11504.
(30) Liu, M.; Li, W.; Qiu, F.; Shi, A.-C. *Macromolecules* **2012**, *45*, 9522–9530.
(31) Daniels, D. R.; McLeish, T. C. B.; Crosby, B. J.; Young, R. N.; Fernyhough, C. M. *Macromolecules* **2001**, *34*, 7025–7033.
(32) McLeish, T. C. B. *Advances in Physics* **2002**, *51*, 1379–1527.
(33) Kapnistos, M.; Vlassopoulos, D.; Roovers, J.; Leal, L. G. *Macromolecules* **2005**, *38*, 7852–7862.
(34) Chambon, P.; Fernyhough, C. M.; Im, K.; Chang, T.; Das, C.; Embery, J.; McLeish, T. C. B.; Read, D. J. *Macromolecules* **2008**, *41*, 5869–5875.
(35) Kapnistos, M.; Kirkwood, K. M.; Ramirez, J.; Vlassopoulos, D.; Leal, L. G. *J. Rheol.* **2009**, *53*, 1133–1153.
(36) Larson, R. G. *Science* **2011**, *333*, 1834–1835.
(37) van Ruymbeke, E.; Lee, H.; Chang, T.; Nikopoulou, A.; Hadjichristidis, N.; Snijkers, F.; Vlassopoulos, D. *Soft Matter* **2014**, *10*, 4762–4777.
(38) Mai, D. J.; Marciel, A. B.; Sing, C. E.; Schroeder, C. M. *ACS Macro Lett.* **2015**, *4*, 446–452.
(39) Jeong, S. H.; Kim, J. M.; Baig, C. *Macromolecules* **2017**, *50*, 4491–4500.
(40) Olvera de la Cruz, M.; Sanchez, I. C. *Macromolecules* **1986**, *19*, 2501–2508.
(41) Grayer, V.; Dormidontova, E. E.; Hadziioannou, G.; Tsitsilianis, C. *Macromolecules* **2000**, *33*, 6330–6339.
(42) Zhang, J.; Schneiderman, D. K.; Li, T.; Hillmyer, M. A.; Bates, F. S. *Macromolecules* **2016**, *49*, 9108–9118.
(43) Gai, Y.; Song, D.-P.; Yavitt, B. M.; Watkins, J. J. *Macromolecules* **2017**, *50*, 1503–1511.

(44) Martinez, H.; Ren, N.; Matta, M. E.; Hillmyer, M. A. *Polym. Chem.* **2014**, *5*, 3507–3532.
(45) Bielawski, C. W.; Grubbs, R. H. *Prog. Polym. Sci.* **2007**, *32*, 1–29.
(46) Leitgeb, A.; Wappel, J.; Slugovc, C. *Polymer* **2010**, *51*, 2927–2946.
(47) Sutthasupa, S.; Shiotsuki, M.; Sanda, F. *Polym. J.* **2010**, *42*, 905–915.
(48) Hong, S. W.; Gu, W.; Huh, J.; Sveinbjornsson, B. R.; Jeong, G.; Grubbs, R. H.; Russell, T. P. *ACS Nano* **2013**, *7*, 9684–9692.
(49) Chang, A. B.; Bates, C. M.; Lee, B.; Garland, C. M.; Jones, S. C.; Spencer, R. K. W.; Matsen, M. W.; Grubbs, R. H. *Proc. Natl. Acad. Sci. U.S.A.* **2017**, *114*, 6462–6467.
(50) Daniel, W. F. M.; Burdynska, J.; Vatankhah-Varnoosfaderani, M.; Matyjaszewski, K.; Paturej, J.; Rubinstein, M.; Dobrynin, A. V.; Sheiko, S. S. *Nat. Mater.* **2016**, *15*, 183–189.
(51) Paturej, J.; Sheiko, S. S.; Panyukov, S.; Rubinstein, M. *Sci. Adv.* **2016**, *2*, e1601478.
(52) Mapas, J. K. D.; Thomay, T.; Cartwright, A. N.; Ilavsky, J.; Rzayev, J. *Macromolecules* **2016**, *49*, 3733–3738.
(53) Bates, F. S.; Fredrickson, G. H. *Annu. Rev. Phys. Chem.* **1990**, *41*, 525–557.
(54) Matsen, M. W. *J. Chem. Phys.* **1996**, *104*, 7758–7764.
(55) Jiang, Y.; Zhang, X.; Miao, B.; Yan, D.; Chen, J. Z. Y. *Soft Matter* **2016**, *12*, 2481–2490.
(56) Elli, S.; Ganazzoli, F.; Timoshenko, E. G.; Kuznetsov, Y. A.; Connolly, R. *J. Chem. Phys.* **2004**, *120*, 6257–6267.
(57) Fredrickson, G. H. *Macromolecules* **1993**, *26*, 2825–2831.
(58) Hsu, H.-P.; Paul, W.; Rathgeber, S.; Binder, K. *Macromolecules* **2010**, *43*, 1592–1601.
(59) Haugan, I. N.; Maher, M. J.; Chang, A. B.; Lin, T.-P.; Grubbs, R. H.; Hillmyer, M. A.; Bates, F. S. *ACS Macro Lett.* **2018**, *7*, 525–530.
(60) Pakula, T.; Zhang, Y.; Matyjaszewski, K.; Lee, H.-i.; Boerner, H.; Qin, S.; Berry, G. C. *Polymer* **2006**, *47*, 7198–7206.
(61) Mpoukouvalas, A.; Li, W.; Graf, R.; Koynov, K.; Matyjaszewski, K. *ACS Macro Lett.* **2013**, *2*, 23–26.
(62) Cai, L.-H.; Kodger, T. E.; Guerra, R. E.; Pegoraro, A. F.; Rubinstein, M.; Weitz, D. A. *Adv. Mater.* **2015**, *27*, 5132–5140.
(63) Dalsin, S. J.; Hillmyer, M. A.; Bates, F. S. *ACS Macro Lett.* **2014**, *3*, 423–427.
(64) Lohse, D. J.; Milner, S. T.; Fetters, L. J.; Xenidou, M.; Hadjichristidis, N.; Mendelson, R. A.; García-Franco, C. A.; Lyon, M. K. *Macromolecules* **2002**, *35*, 3066–3075.
(65) Liang, H.; Cao, Z.; Wang, Z.; Sheiko, S. S.; Dobrynin, A. V. *Macromolecules* **2017**, *50*, 3430–3437.
(66) Cao, Z.; Daniel, W. F. M.; Vatankhah-Varnosfaderani, M.; Sheiko, S. S.; Dobrynin, A. V. *Macromolecules* **2016**, *49*, 8009–8017.
(67) Saariaho, M.; Szleifer, I.; Ikkala, O.; Brinke, G. t. *Macromol. Theory Simul.* **1998**, *7*, 211–216.
(68) Williams, M. L.; Landel, R. F.; Ferry, J. D. *J. Am. Chem. Soc.* **1955**, *77*, 3701–3707.
(69) van Gurp, M.; Palmen, J. *Rheology Bulletin* **1998**, *67*, 5.

(70) Hu, M.; Xia, Y.; McKenna, G. B.; Kornfield, J. A.; Grubbs, R. H. *Macromolecules* **2011**, *44*, 6935–6943.
(71) Dalsin, S. J.; Hillmyer, M. A.; Bates, F. S. *Macromolecules* **2015**, *48*, 4680–4691.
(72) Tsukahara, Y.; Namba, S.-i.; Iwasa, J.; Nakano, Y.; Kaeriyama, K.; Takahashi, M. *Macromolecules* **2001**, *34*, 2624–2629.
(73) Graessley, W. W. *Macromolecules* **1982**, *15*, 1164–1167.
(74) Kempf, M.; Ahirwal, D.; Cziep, M.; Wilhelm, M. *Macromolecules* **2013**, *46*, 4978–4994.
(75) Lin, Y.; Zheng, J.; Yao, K.; Tan, H.; Zhang, G.; Gong, J.; Tang, T.; Xu, D. *Polymer* **2015**, *59*, 252–259.